



ELSEVIER

Contents lists available at ScienceDirect

Comptes Rendus Geoscience

www.sciencedirect.com



Petrology, Geochemistry

Presumed magnetic biosignatures observed in magnetite derived from abiotic reductive alteration of nanogoethite



Jessica L. Till^{a,b,c}, Yohan Guyodo^a, France Lagroix^{b,*}, Guillaume Morin^a,
Nicolas Menguy^a, Georges Ona-Nguema^a

^a Institut de minéralogie, de physique des matériaux et de cosmochimie (IMPMC), Sorbonne Universités–UMPC, CNRS UMR 7590, Muséum national d'histoire naturelle, IRD UMR 206, 4, place Jussieu, 75005 Paris, France

^b Institut de physique du globe de Paris, Sorbonne Paris Cité, université Paris-Diderot, UMR 7154 CNRS, 1, rue Jussieu, 75005 Paris, France

^c Institute of Earth Sciences, University of Iceland, Askja, 7, Sturlugata, 101 Reykjavik, Iceland

ARTICLE INFO

Article history:

Received 1st February 2017

Accepted after revision 2 February 2017

Available online 10 March 2017

Handled by Philippe Cardin

Keywords:

Magnetite

Magnetosomes

Inorganic alteration

Nano-goethite

Magnetism-based biosignature

ABSTRACT

The oriented chains of nanoscale Fe-oxide particles produced by magnetotactic bacteria are a striking example of biomineralization. Several distinguishing features of magnetite particles that comprise bacterial magnetosomes have been proposed to collectively constitute a biosignature of magnetotactic bacteria (Thomas-Keprta et al., 2001). These features include high crystallinity, chemical purity, a single-domain magnetic structure, well-defined crystal morphology, and arrangement of particles in chain structures. Here, we show that magnetite derived from the inorganic breakdown of nanocrystalline goethite exhibits magnetic properties and morphologies remarkably similar to those of biogenic magnetite from magnetosomes. During heating in reducing conditions, oriented nanogoethite aggregates undergo dehydroxylation and transform into stoichiometric magnetite. We demonstrate that highly crystalline single-domain magnetite with euhedral grain morphologies produced abiogenically from goethite meets several of the biogenicity criteria commonly used for the identification of magnetofossils. Furthermore, the suboxic conditions necessary for magnetofossil preservation in sediments are conducive to the reductive alteration of nanogoethite, as well as the preservation of detrital magnetite originally formed from goethite. The findings of this study have potential implications for the identification of biogenic magnetite, particularly in older sediments where diagenesis commonly disrupts the chain structure of magnetosomes. Our results indicate that isolated magnetofossils cannot be positively distinguished from inorganic magnetite on the basis of their magnetic properties and morphology, and that intact chain structures remain the only reliable distinguishing feature of fossil magnetosomes.

© 2017 Académie des sciences. Published by Elsevier Masson SAS. All rights reserved.

1. Introduction

Magnetotactic bacteria (MTB) are a diverse group of microbes that produce chains of magnetic nanoparticles called magnetosomes for the purpose of navigation. MTB

have been identified in an extensive variety of freshwater and marine environments (Favre and Schuler, 2008), and the preserved magnetosome components of such bacteria, also known as magnetofossils, have been identified in sediments dating at least as far back as the Cretaceous (Montgomery et al., 1998). The stoichiometric magnetite that comprises most bacterial magnetosomes consistently exhibits certain features, including a high degree of crystallinity with few crystallographic defects,

* Corresponding author.

E-mail addresses: jtill@hi.is (J.L. Till), lagroix@ipgp.fr (F. Lagroix).

high chemical purity, a single-domain magnetic structure, well-defined crystal morphology, and arrangement of particles in chain structures (Kopp and Kirschvink, 2008). These collective attributes have been proposed as a biosignature of magnetotactic bacteria and have been applied as criteria for the identification of magnetofossils in sediments, sedimentary rocks, and even meteorites (Thomas-Keprta et al., 2001).

While all of the above criteria are typically observed in cultured strains of MTB and live bacteria sampled from modern aqueous environments, studies of older sediments often fail to observe intact chain structures in fossil magnetosomes due to the collapse and the disaggregation of the chains either through diagenesis or by laboratory protocols of magnetic mineral extraction for microscopic investigation. In some cases, methods such as ferromagnetic resonance or low-temperature magnetic measurements can be used to infer the presence of magnetic chain structures (Weiss et al., 2004a). However, many studies on ancient sediments rely on the microscopic observation of magnetic extracts, combined with the analysis of sediment magnetic properties to detect single-domain (SD) magnetite (e.g., Abrajevitch et al., 2015; Larrasoana et al., 2014; Savian et al., 2016).

Although the inorganic magnetite fraction in many sediments is not usually considered to include a significant amount of SD material, recent studies have recognized that certain types of detrital particles, such as magnetic inclusions in silicate minerals, are widespread and important contributors to fine-particle magnetism in sediments (Chang et al., 2016b). Additionally, this type of detrital SD magnetite can obscure the rock magnetic signatures of the biogenic magnetite fraction (Chang et al., 2016a). A number of earlier studies demonstrated that various inorganic processes can produce magnetite with certain characteristic morphologies of biogenic magnetite to explain the occurrence of SD magnetite in the ALH84001 Martian meteorite (Barber and Scott, 2002; Bradley et al., 1998; Golden et al., 2004). However, inorganic processes are rarely invoked to explain the biogenic characteristics of SD magnetite in terrestrial environments. Rather it is assumed that because MTB are widespread in modern aqueous environments, they are likely to have been widespread throughout much of Earth's history and hence much ancient sediment may be expected to carry magnetic signatures of magnetofossils. Here, we describe various magnetosome-like properties of nanoscale magnetite particles produced by inorganic alteration of nanocrystalline goethite. We propose that magnetite produced by this reaction pathway could potentially contribute to the SD magnetite signals in sediment magnetic properties that are commonly attributed to biogenic magnetite.

The Fe-oxyhydroxide goethite occurs in nanocrystalline form in a wide range of soils, aeolian material, and lake and marine sediments (van der Zee et al., 2003). In many sedimentary systems, it is the dominant substrate available for Fe-redox reactions (Hansel et al., 2004; van der Zee et al., 2003). Nanogoethite is predicted to be thermodynamically unstable with respect to the dehydroxylation to Fe-oxide at ambient temperatures on geologic time scales (Diakonov et al., 1994; Langmuir,

1971), although the kinetics are sufficiently slow so that no reaction occurs below 100 °C on laboratory time scales (Diakonov et al., 1994). Recently, a study by Till et al. (2015) reported that nanogoethite readily alters to sub-micron magnetite under reducing conditions upon moderate heating ($T = 210\text{--}270$ °C). They identified a two-step process involving dehydroxylation of goethite to nanohematite, and subsequent rapid reduction and recrystallization of nanohematite to fine-grained magnetite. Here, we analyze the magnetite produced in these experiments in detail using transmission electron microscopy (TEM) and rock magnetic measurements, and describe the results below.

2. Procedures

2.1. Synthesis

Synthetic nanogoethite was produced using the protocol outlined in Schwertmann and Cornell (1991). A 0.05-M solution of $\text{FeCl}_2 \cdot 4\text{H}_2\text{O}$ was prepared in a glove box using deoxygenated water and was mixed with a 1 M NaHCO_3 solution. After removing the mixed solution from the glove box, a constant flow of air was bubbled through the resulting suspension, which was continuously agitated and became oxidized over 48 h. The goethite precipitate was separated by centrifuging and rinsing with ultrapure (MilliQ) water several times and dried in a vacuum desiccator. The resulting goethite particles are around 10 nm by 50 nm in size, and consist of well-oriented aggregates of crystallites with crystallite sizes around 6 nm (Till et al., 2015).

2.2. Characterization

The starting material and reaction products were characterized by Rietveld refinement of the X-ray diffraction (XRD) powder patterns and imaged by high-resolution transmission electron microscopy on a JEOL 2100F microscope with a field-emission gun at a 200-kV accelerating voltage. Electron diffraction patterns were calculated by fast Fourier transforms of high-resolution images. Samples for magnetic measurements were prepared using small amounts of undiluted sample powders packed in gelatin capsules. Low-temperature magnetic measurements of saturation isothermal remanent magnetization (SIRM) curves measured on warming from 10 K after field-cooling (FC) in a 2.5-T field or cooling in zero-field (ZFC), were made on a Quantum Designs Magnetic Properties Measurement System (MPMS XL-5 with EverCool). $\delta_{\text{FC}}/\delta_{\text{ZFC}}$ ratios were calculated as $\delta = (M_{\text{irm}}[80] - M_{\text{irm}}[150])/M_{\text{irm}}(80)$, where M is the value of the magnetic remanence at 80 K or 150 K upon warming after either FC or ZFC pre-treatment. First-order reversal curve (FORC) distributions and hysteresis loops were measured on a Princeton Measurements Corporation vibrating sample magnetometer (VSM) at room temperature. FORC measurements used a maximum field of 0.3 T, which is greater than the magnetic saturating field of the samples, and a field increment of 1 mT. FORC diagrams

Table 1
Room-temperature hysteresis parameters and experimental conditions for altered samples.

Sample	Temp (°C)	Heating time (min)	M_s (A·m ² /kg)	M_r (A·m ² /kg)	H_c (mT)
G02	250	150	49	15	17
G03	230	150	4.3	1.1	10
G04	210	155	3.8	0.59	4.6
G05	270	75	65	18	19

were processed and plotted with the FORCinel software package (Harrison and Feinberg, 2008) using the VARIFORC smoothing protocol (Egli, 2013).

2.3. Alteration experiments

Alteration experiments were performed by heating synthetic nanogoethite powder at temperatures between 210 and 270 °C for up to 2.5 h in a constant flow of a 20%–80% CO–CO₂ gas mixture. The furnace used for heating experiments was enclosed inside an Ar-filled glove box, and samples were prepared and maintained under anoxic conditions to minimize sample oxidation. Magnetic characterization was performed immediately after each alteration experiment. Conditions for each experimental run as well as detailed results of XRD and other magnetic measurements were reported by Till et al. (2015) and are summarized here (Table 1).

3. Results

3.1. Magnetite morphology

Based on previously reported XRD data for the altered samples, the mean magnetite grain size is around 30 nm in samples G02, G03, and G05 (Till et al., 2015). Sample G05 did not contain any detectable hematite or goethite. TEM images of magnetite in sample G05 reveal that the majority of grains are rounded and elongated, ranging from about 20 to 60 nm in width (Fig. 1a–c). Although many grains have irregular or non-distinct shapes, a significant portion exhibits striking similarities to magnetite particles found in magnetosomes. Short-chain-like arrangements of particles were also occasionally observed in TEM images (Fig. 1d and e), although the spontaneously formed chain configurations in our samples can be distinguished from chains formed by MTB by the lack of repeated regular grain shapes and close spacing of the particles. Fig. 2a and b display examples of elongated, tapered particles that resemble bullet-shaped magnetosome particles found in certain MTB strains (Kopp and Kirschvink, 2008). A number of equant and slightly elongated euhedral particles were found whose shapes are consistent with various reported prismatic or cubo-octahedral magnetosome morphologies (Fig. 2c–g). The high-resolution TEM images in Fig. 2 are accompanied by simulated diffraction patterns for individual grains that were produced by Fourier transforms of the images. The planar spacing and angle values in the simulated diffraction patterns can all be indexed to the

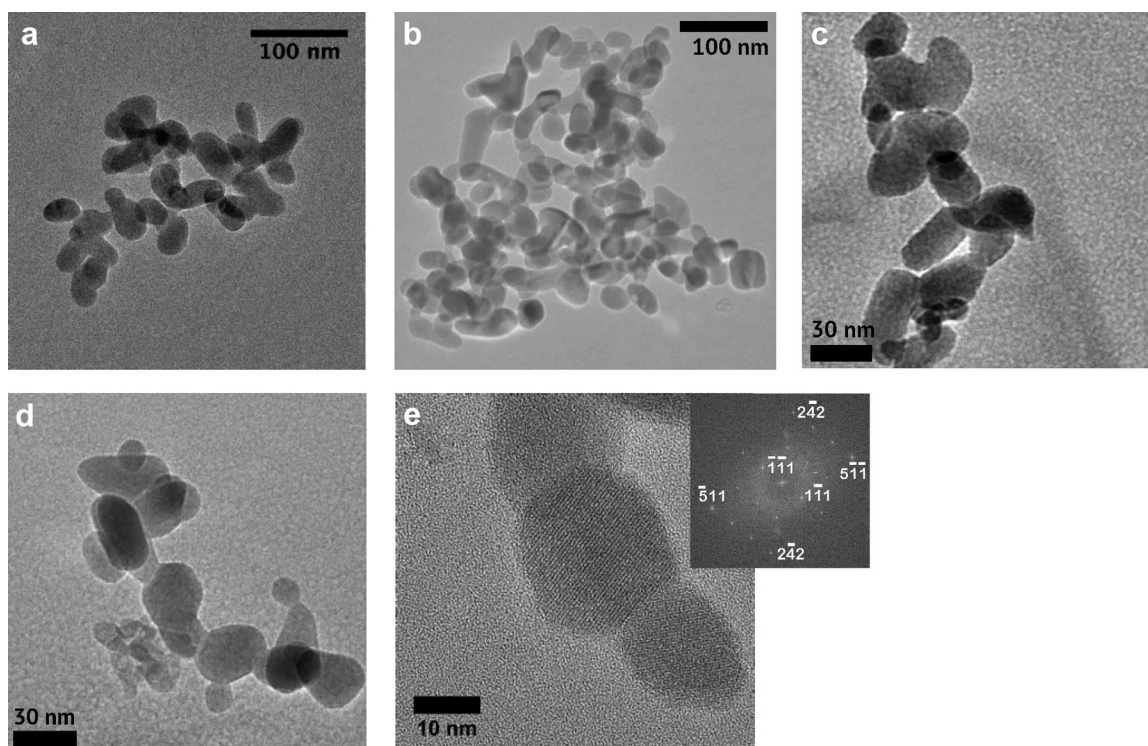


Fig. 1. Examples of magnetite produced by reductive dehydroxylation of nanogoethite aggregates imaged by TEM. a–c: clusters of magnetite particles demonstrating dominantly rounded, elongated shapes; d and e: magnetite particles arranged in short irregular chains. The inset in (e) is a simulated electron diffraction pattern of the grain in the center of the image.

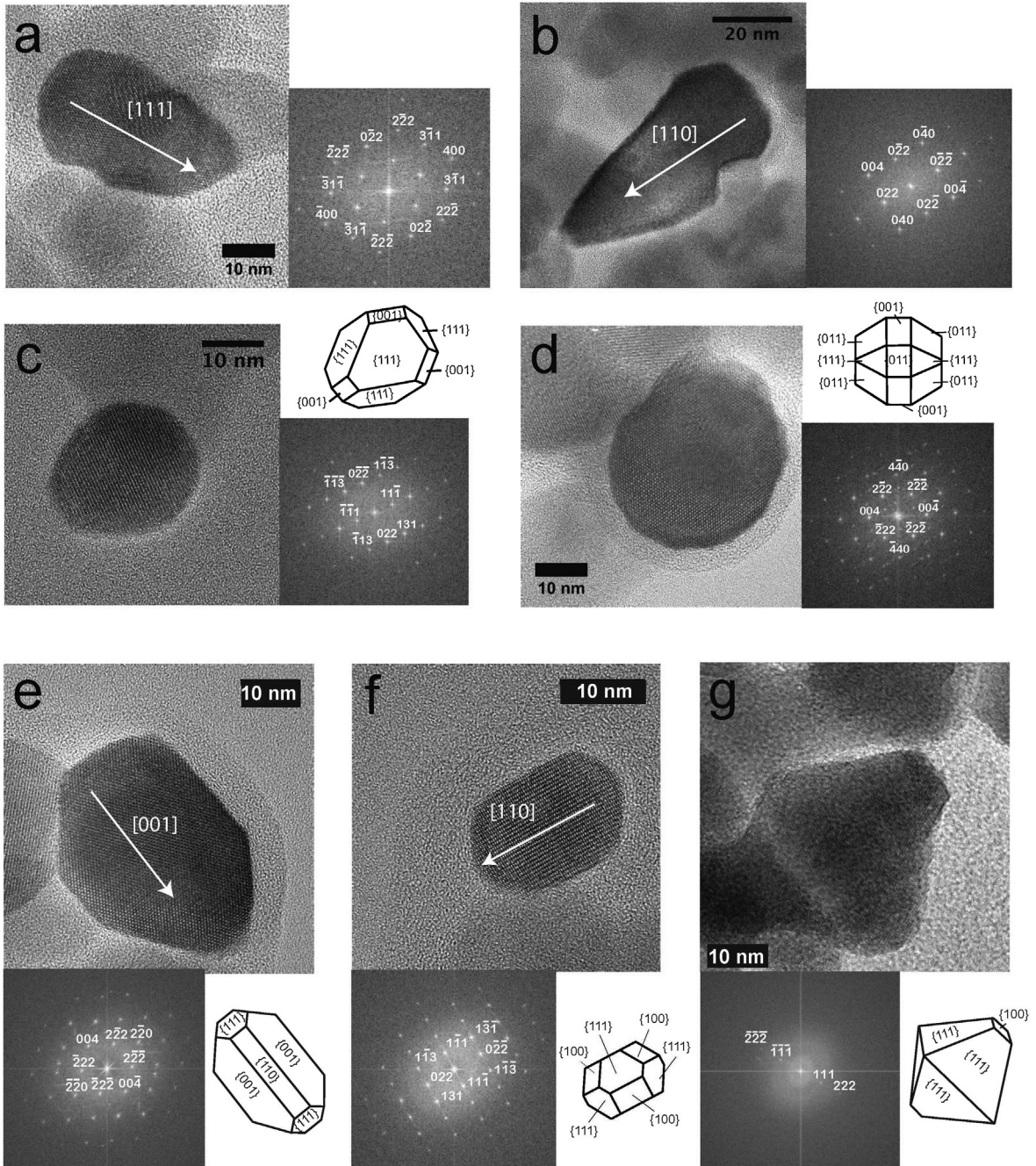


Fig. 2. High-resolution TEM images of highly crystalline euhedral magnetite grains and schematic illustrations of idealized crystal morphologies consistent with the grain orientations. a and b: elongated tapered magnetite grains resembling bullet-shaped magnetosome particles; c and d: equant magnetite grains approximately cubo-octahedral morphologies; e–g: highly euhedral magnetite grains with prismatic or cubo-octahedral morphologies. Insets are simulated electron diffraction patterns for particles in each image.

magnetite crystal structure. The magnetite crystals are consistently highly crystalline and free of defects. Elongated particles have long axis orientations parallel to either the $\langle 100 \rangle$, $\langle 110 \rangle$, or $\langle 111 \rangle$ directions. Although magnetosomes with prismatic or cubo-octahedral morphologies are most commonly observed to have elongations along the $\langle 111 \rangle$ easy axis of magnetization (Favre and Schuler, 2008), bullet-shaped magnetosomes can be

elongated along any of the three principal long axes, as is observed in our samples (e.g., Pósfai et al., 2013).

3.2. Magnetic properties

To examine the distribution of magnetic domain states and degree of magnetostatic interactions in nanogoethite-derived magnetite, first-order reversal curve diagrams

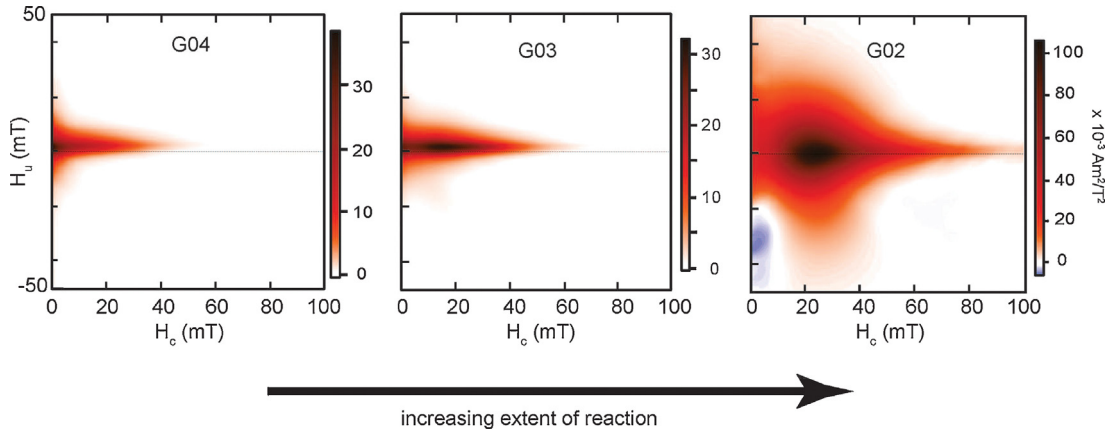


Fig. 3. FORC distribution diagrams for altered goethite G04, G03, and G02 samples representing different stages of magnetite growth during transformation from left to right. Smoothing parameters of $s_{c0} = 7$, $s_{b0} = 5$, $s_{c1} = s_{b1} = 12$ and $\lambda_c = \lambda_b = 0.1$ have been applied to each FORC diagram.

were obtained for altered goethite samples containing magnetite in various stages of the reaction. Partially-reacted G04 and G03 samples containing approximately 4 and 5 wt% magnetite, based on saturation magnetization (M_s) values in Table 1 and the theoretical value of 92 A·m²/kg for stoichiometric magnetite (Dunlop and Özdemir, 1997), exhibit relatively small interaction fields and a high-coercivity (H_c) “tail” extending along the central horizontal axis (Fig. 3). These samples contain a high proportion of superparamagnetic (SP) grains based on the high frequency-dependence of susceptibility values at room temperature reported by Till et al. (2015), as well as relatively low H_c values (Table 1). The FORC distributions of these samples reflect a grain size distribution consisting of a mixture of superparamagnetic and weakly interacting small SD magnetite grains. Magnetite-rich samples, G02 and G05 with approximately 53 and 71 wt% magnetite respectively, display a localized peak with a broader vertical spread indicating higher magnetostatic interaction fields (H_u) and overall higher coercivities, again including a high-coercivity tail with low interaction fields (Fig. 3). The teardrop-shaped FORC pattern for sample G02 and its lobe extending along the negative H_u axis is characteristic of interacting SD magnetite and similar distributions have

been observed for experimentally disaggregated magnetosome particles (Kopp and Kirschvink, 2008; Moskowitz et al., 1993), for some magnetofossil-bearing sediments (Roberts et al., 2012) and in simulations of FORC diagrams for randomly packed randomly oriented uniaxial magnetite particles (Harrison and Lascu, 2014). The shape of the interaction fields in FORC distributions for samples G02 and G05 are also distinct from those of synthetic pseudo-single-domain magnetite, which exhibits much higher H_u values (e.g., Till et al., 2010).

Pure intact magnetosome chains and sediments dominated by intact magnetofossils typically display a narrow horizontal central ridge signifying non-interacting SD magnetite in FORC diagrams. In natural sediments, the addition of strongly interacting detrital magnetite can mask the central ridge, requiring certain measurement procedures to isolate the biogenic component of magnetization (Egli et al., 2010). The high-coercivity tails seen for our samples resemble the central ridge displayed by biogenic magnetite, but do not represent a separate mineral component; rather they likely represent relatively isolated magnetite particles in a matrix of incompletely reacted nanohematite that are sufficiently dispersed to be weakly interacting. Interaction effects may be further

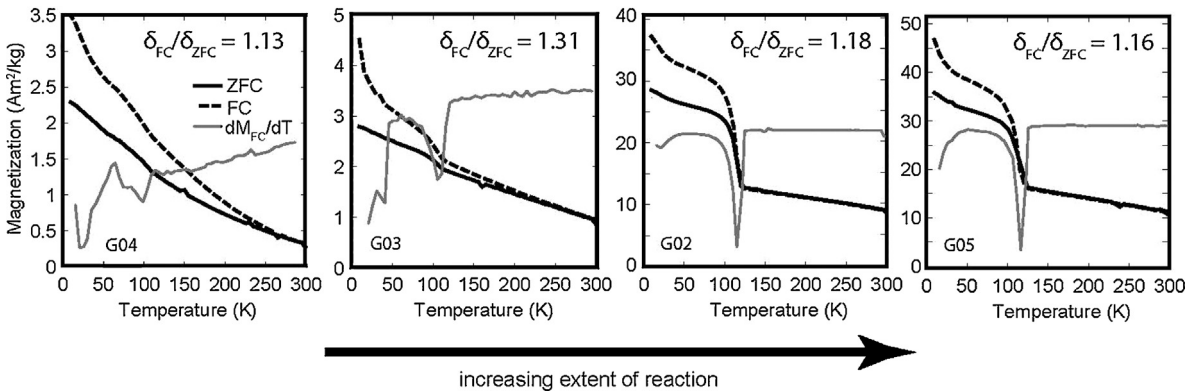


Fig. 4. Measurements of low-temperature saturation isothermal magnetic remanence (SIRM) measured on warming from 10 K after zero-field cooling (ZFC) or field cooling (FC) in a 2.5-T field for various stages of the reductive alteration products of nano-goethite. Solid grey lines represent derivatives of FC remanence curves with local minima indicating the temperature of the Verwey transition.

reduced for highly dispersed magnetite particles in sedimentary material, in contrast to the high magnetite concentrations in our measured samples. Previous studies have demonstrated that well-dispersed, fine inorganic magnetite can also display features of non-interacting SD particles in FORC diagrams (Egli et al., 2010), including pedogenic Fe-oxides in soils (Geiss et al., 2008). The close similarities between the FORC distributions for our samples in Fig. 2 and those reported for magnetofossil-bearing sediments (e.g., Roberts et al., 2012) suggest that the potential presence of nanogoethite-derived magnetite in natural settings may confound the identification of magnetofossils.

The Moskowitz test (Moskowitz et al., 1993) is a commonly used magnetic measurement for detecting intact magnetosome chains. The δ_{FC}/δ_{ZFC} ratio is based on the loss in remanence on warming through the Verwey crystallographic transition around 120 K (Verwey, 1939) and is greater than 2 for intact magnetosome chains, while values between 1 and 2 indicate that SD magnetite is present in other forms, including disaggregated or oxidized magnetosomes. δ_{FC}/δ_{ZFC} values for our magnetite-bearing samples are between 1.1 and 1.3 (Fig. 4). These values fall in the same range as the magnetite-bearing carbonate globules in Martian meteorite ALH84001 (Weiss et al., 2004b), experimentally disaggregated magnetosomes (Li et al., 2012), and marine sediment cores inferred to contain partially oxidized magnetofossils (Housen and Moskowitz, 2006).

The sharpness of the Verwey transition around 120 K for the nearly pure magnetite end-product (sample G05; Fig. 4) indicates a high degree of oxygen stoichiometry and the absence of substitutional impurities (Weiss et al., 2004b), as expected from the high purity of the starting goethite material. Although natural goethite commonly occurs in aluminous forms with up to 30 mol% Al substitution (Tardy and Nahon, 1985), the stabilizing effect of aluminum (Ruan and Gilkes, 1995) suggests that Al-free goethite will alter to magnetite more readily and that Al-substituted magnetite produced by this pathway should be less common. Despite the success of some studies in producing magnetosomes doped with small amounts of metals (e.g., Prozorov et al., 2014), cation substitution in magnetite remains an important counter-indicator of biogenicity (Amor et al., 2015), and the occurrence of aluminum substitution in particular would strongly support an origin from detrital or authigenic goethite.

4. Discussion and conclusions

Table 1 indicates that altered nanogoethite samples heated at higher temperatures (250–270 °C) contain more magnetite than samples from lower-temperature experiments (210–230 °C) for equivalent heating times. For thermally-activated processes, higher temperatures result in enhanced reaction kinetics that can be used to simulate the effects of longer reaction times at lower temperatures. Therefore, if the same nanogoethite transformation mechanisms operate over a given temperature range, i.e. dehydroxylation followed by nanohematite reduction and

recrystallization, then we predict that samples heated at lower temperatures for longer durations would eventually produce magnetite similar to the higher-temperature samples, G02 and G05. With increasing time, the inferred transformation process involves nucleation of initially isolated SP magnetite particles that coalesce and grow into stable SD-sized particles (Till et al., 2015) approximately equal in size to the original nanogoethite aggregates. For the pure nanogoethite starting material used here, some sintering of adjacent particles is also possible, and higher temperatures and/or longer reaction times may promote further grain growth through sintering. However, in natural sediments or soils where goethite is typically dispersed among other phases, the size of secondary magnetite particles that can form will be limited by the original size of the goethite particles or aggregates.

Till et al. (2015) identified various pathways by which altered nanogoethite may contribute nanoscale magnetic particles to sediments and soils, including thermal alteration by low-grade metamorphism, diagenesis in marine sediments and by wildfire in soils. Elevated temperatures generated during deep burial of meta-sediments will promote the breakdown of goethite and may lead to the formation of authigenic magnetite under reducing conditions. The stability of goethite in anoxic sediments at ambient temperatures is unknown, but it is unlikely to be stable under reducing diagenetic conditions. The possibility of in-situ magnetite formation from low-temperature goethite alteration in sedimentary settings should be further investigated. This is especially true given that current knowledge of the stability of nanoparticles of goethite and other iron oxides and hydroxides is even sparser than for coarser-grained phases (Lagroix et al., 2016), yet it is crucially important for magnetism-based interpretations of past climate events, such as the Paleocene–Eocene Thermal Maximum (PETM) (e.g. Maxbauer et al., 2016).

Production of fine magnetic particles and soil magnetic enhancement alteration has been documented to result from goethite alteration during wildfire in various soil types (Anand and Gilkes, 1987; Clement et al., 2011; Ketterings et al., 2000; Nornberg et al., 2009). Nanoparticles produced by fire have high mobility due to both increased surface runoff and sediment delivery to lake catchments (Smith et al., 2013) and from increased wind erosion and aeolian transport following wildfire events (Whicker et al., 2002). These processes represent pathways by which detrital goethite-derived magnetite may enter lake and marine sediments, particularly marine settings with substantial continental inputs from aeolian deposition or submarine fans. Aeolian sediments and detrital material from weathered igneous formations have previously been recognized as potential sources of SD magnetite (Roberts et al., 2012). Although some careful studies have found certain distinguishing factors, such as double Verwey transitions, which can isolate signals from detrital and biogenic SD magnetite (Chang et al., 2016a), other sediment magnetism studies rely on magnetic signatures such as weak magnetostatic interactions, narrow coercivity and grain size distributions, and magnetosome-like crystal morphologies to identify biogenic magnetite. Our

findings demonstrate that inorganic magnetite particles can exhibit many of the same magnetic signatures and crystal morphologies that are characteristic of disaggregated magnetosomes and isolated magnetofossils in sediments.

Further complicating the problem of magnetofossil identification is that the conditions suitable for the preservation of inorganic SD magnetite in sediments should be identical to those required for the preservation of magnetofossils. Namely, anoxic or suboxic conditions are required to inhibit oxidation, but must not be so reducing that fine magnetite particles begin to dissolve. Reliable identification of suspected magnetofossils should address the robustness measures outlined by Kopp and Kirschvink (2008), including the assessment of high-quality paleomagnetic data, to rule out the possibility of secondary magnetizations that would result from the authigenic growth of SD magnetite. Some types of detrital SD magnetite that share the physical characteristics of biogenic magnetite will also produce high-quality paleomagnetic records, but will not meet the key criterion of long, intact chain structures detected either by direct microscopic observation or by various indirect tests such as ferromagnetic resonance, the Moskowitz test (Moskowitz et al., 1993) or the more recently developed and tested thermal fluctuation tomography method (Wang et al., 2013).

Our findings underscore the need for careful characterization of potential magnetofossils and reinforce the assertions of previous studies (Barber and Scott, 2002; Golden et al., 2004; Wang et al., 2015) that cubo-octahedral morphologies in single-domain magnetite are not strictly unique to MTB magnetosomes. Currently, the presumed diagnostic single ridge feature of FORC distributions requires additional supporting evidence, which researchers have sought to obtain from TEM images, invariably performed on magnetic extracts. However, even the most rigorous protocol may lead to the extraction of only a few percent of the total population of magnetic particles (e.g., Wang et al., 2013), thus providing a biased representation. We contend that the observation of isolated euhedral magnetite particles and magnetic properties associated with SD particles in sediments are not sufficient evidence for a biogenic origin. Given the widespread occurrence of nanocrystalline goethite in nature, its role as a potential precursor to sedimentary magnetite should be considered in future studies.

Acknowledgments

This work was supported by the “Agence nationale de la recherche” (France) under project 2010-BLAN-604-01. Dennis Kent and Joshua Feinberg are thanked for their constructive reviews. This is ICPG contribution 3826.

References

- Abrajewitch, A., Font, E., Florindo, F., Roberts, A.P., 2015. Asteroid impact vs Deccan eruptions: the origin of low magnetic susceptibility beds below the Cretaceous-Paleogene boundary revisited. *Earth Planet. Sci. Lett.* 430, 209–223.
- Amor, M., Busigny, V., Durand-Dubief, M., Tharaud, M., Ona-Nguema, G., Gelabert, A., Alphandery, E., Menguy, N., Benedetti, M.F., Chebbi, I., Guyot, F., 2015. Chemical signature of magnetotactic bacteria. *Proc. Natl. Acad. Sci. U. S. A.* 112 (6), 1699–1703.
- Anand, R.R., Gilkes, R.J., 1987. The association of maghemite and corundum in Darling Range laterites, Western Australia. *Austr. J. Soil Res.* 25 (3), 303–311.
- Barber, D.J., Scott, E.R.D., 2002. Origin of supposedly biogenic magnetite in the Martian meteorite Allan Hills 84001. *Proc. Natl. Acad. Sci. U. S. A.* 99 (10), 6556–6561.
- Bradley, J.P., McSween Jr., H.Y., Harvey, R.P., 1998. Epitaxial growth of nanophase magnetite in Martian meteorite Allan Hills 84001: implications for biogenic mineralization. *Meteor. Planet. Sci.* 33 (4), 765–773.
- Chang, L., Heslop, D., Roberts, A.P., Rey, D., Mohamed, K.J., 2016a. Discrimination of biogenic and detrital magnetite through a double Verwey transition temperature. *J. Geophys. Res. Solid Earth* 121 (1), 3–14.
- Chang, L., Roberts, A.P., Heslop, D., Hayashida, A., Li, J., Zhao, X., Tian, W., Huang, Q., 2016b. Widespread occurrence of silicate-hosted magnetic mineral inclusions in marine sediments and their contribution to paleomagnetic recording. *J. Geophys. Res. Solid Earth* 121 (12), 8415–8431.
- Clement, B.M., Javier, J., Sah, J.P., Ross, M.S., 2011. The effects of wildfires on the magnetic properties of soils in the Everglades. *Earth Surf. Proc. Land.* 36 (4), 460–466.
- Diakonov, I., Khodakovskiy, I., Schott, J., Sergeeva, E., 1994. Thermodynamic properties of iron-oxides and hydroxides. 1. Surface and bulk thermodynamic properties of goethite (alpha-FeOOH) up to 500 K. *Eur. J. Mineral.* 6 (6), 967–983.
- Dunlop, D.J., Özdemir, Ö., 1997. *Rock magnetism: fundamentals and frontiers*. Cambridge studies in magnetism. Cambridge University Press, 573 p.
- Egli, R., 2013. VARIFORC: an optimized protocol for calculating non-regular first-order reversal curve (FORC) diagrams. *Global Planet. Change* 110, 302–320.
- Egli, R., Chen, A.P., Winklhofer, M., Kodama, K.P., Hornig, C.S., 2010. Detection of noninteracting single domain particles using first-order reversal curve diagrams. *Geochem. Geophys. Geosyst.* 11, <http://dx.doi.org/10.1029/2009GC002916>.
- Faivre, D., Schuler, D., 2008. Magnetotactic bacteria and magnetosomes. *Chem. Rev.* 108 (11), 4875–4898.
- Geiss, C.E., Egli, R., Zanner, C.W., 2008. Direct estimates of pedogenic magnetite as a tool to reconstruct past climates from buried soils. *J. Geophys. Res. Solid Earth* 113 (B11).
- Golden, D.C., Ming, D.W., Morris, R.V., Brearley, A., Lauer, H.V., Treiman, A.H., Zolensky, M.E., Schwandt, C.S., Lofgren, G.E., McKay, G.A., 2004. Evidence for exclusively inorganic formation of magnetite in Martian meteorite ALH84001. *Am. Mineral.* 89 (5–6), 681–695.
- Hansel, C.M., Benner, S.G., Nico, P., Fendorf, S., 2004. Structural constraints of ferric (hydr)oxides on dissimilatory iron reduction and the fate of Fe(II). *Geochim. Cosmochim. Acta* 68 (15), 3217–3229.
- Harrison, R.J., Feinberg, J.M., 2008. FORCinel: an improved algorithm for calculating first-order reversal curve distributions using locally weighted regression smoothing. *Geochem. Geophys. Geosyst.* 9, <http://dx.doi.org/10.1029/2008GC001987>.
- Harrison, R.J., Lascu, I., 2014. FORCulator: a micromagnetic tool for simulating first-order reversal curve diagrams. *Geochem. Geophys. Geosyst.* 15 (12), 4671–4691.
- Housen, B.A., Moskowitz, B.M., 2006. Depth distribution of magnetofossils in near-surface sediments from the Blake/Bahama Outer Ridge, western North Atlantic Ocean, determined by low-temperature magnetism. *J. Geophys. Res. Biogeosci.* 111 (G1).
- Ketterings, Q.M., Bigham, J.M., Laperche, V., 2000. Changes in soil mineralogy and texture caused by slash-and-burn fires in Sumatra, Indonesia. *Soil Sci. Soc. Am. J.* 64 (3), 1108–1117.
- Kopp, R.E., Kirschvink, J.L., 2008. The identification and biogeochemical interpretation of fossil magnetotactic bacteria. *Earth-Sci. Rev.* 86 (1–4), 42–61.
- Lagroix, F., Banerjee, S.K., Jackson, M.J., 2016. Geological occurrences and relevance of iron oxides. In: Faivre, F. (Ed.), *Iron oxides. From nature to applications*. Wiley-VCH, Weinheim, Germany, pp. 9–29.
- Langmuir, D., 1971. Particle size effect of the reaction goethite = hematite + water. *Am. J. Sci.* 271, 147–156.
- Larrasoana, J.C., Liu, Q.S., Hu, P.X., Roberts, A.P., Mata, P., Civis, J., Sierro, F.J., Perez-Asensio, J.N., 2014. Paleomagnetic and paleoenvironmental implications of magnetofossil occurrences in late Miocene marine sediments from the Guadalquivir Basin, SW Spain. *Front. Microbiol.* 5.
- Li, J.H., Wu, W.F., Liu, Q.S., Pan, Y.X., 2012. Magnetic anisotropy, magnetostatic interactions and identification of magnetofossils. *Geochem. Geophys. Geosyst.* 13, <http://dx.doi.org/10.1029/2012GC004384>.
- Maxbauer, D.P., Feinberg, J.M., Fox, D.L., Clyde, W.C., 2016. Magnetic minerals as recorders of weathering, diagenesis, and paleoclimate:

- a core-outcrop comparison of Paleocene–Eocene paleosols in the Bighorn Basin, WY, USA. *Earth Planet. Sci. Lett.* 452, 15–26.
- Montgomery, P., Hailwood, E.A., Gale, A.S., Burnett, J.A., 1998. The magnetostratigraphy of Coniacian–Late Campanian chalk sequences in southern England. *Earth Planet. Sci. Lett.* 156 (3–4), 209–224.
- Moskowitz, B.M., Frankel, R., Bazylinski, D., 1993. Rock magnetic criteria for the detection of biogenic magnetite. *Earth Planet. Sci. Lett.* 120, 283–300.
- Nornberg, P., Vendelboe, A.L., Gunnlaugsson, H.P., Merrison, J.P., Finster, K., Jensen, S.K., 2009. Comparison of the mineralogical effects of an experimental forest fire on a goethite/ferrihydrate soil with a topsoil that contains hematite, maghemite and goethite. *Clay Miner.* 44 (2), 239–247.
- Pósfai, M., Lefèvre, C.T., Trubitsyn, D., Bazylinski, D.A., Frankel, R.B., 2013. Phylogenetic significance of composition and crystal morphology of magnetosome minerals. *Front. Microbiol.* 4, 344.
- Prozorov, T., Perez-Gonzalez, T., Valverde-Tercedor, C., Jimenez-Lopez, C., Yebra-Rodriguez, A., Kornig, A., Faivre, D., Mallapragada, S.K., Howse, P.A., Bazylinski, D.A., Prozorov, R., 2014. Manganese incorporation into the magnetosome magnetite: magnetic signature of doping. *Eur. J. Mineral.* 26 (4), 457–471.
- Roberts, A.P., Chang, L., Heslop, D., Florindo, F., Larrasoana, J.C., 2012. Searching for single domain magnetite in the “pseudo-single-domain” sedimentary haystack: Implications of biogenic magnetite preservation for sediment magnetism and relative paleointensity determinations. *J. Geophys. Res. Solid Earth* 117 .
- Ruan, H.D., Gilkes, R.J., 1995. Dehydroxylation of aluminous goethite – unit-cell dimensions, crystal size and surface-area. *Clays Clay Miner.* 43 (2), 196–211.
- Savian, J.F., Jovane, L., Giorgioni, M., Iacoviello, F., Rodelli, D., Roberts, A.P., Chang, L., Florindo, F., Sprovieri, M., 2016. Environmental magnetic implications of magnetofossil occurrence during the Middle Eocene Climatic Optimum (MECO) in pelagic sediments from the equatorial Indian Ocean. *Palaeogeogr. Palaeoclimatol. Palaeoecol.* 441, 212–222.
- Schwertmann, U., Cornell, R.M., 1991. *Iron oxides in the laboratory: preparation and characterization*. VCH Publishers, New York, 137 p.
- Smith, H.G., Blake, W.H., Owens, P.N., 2013. Discriminating fine sediment sources and the application of sediment tracers in burned catchments: a review. *Hydrol. Proc.* 27 (6), 943–958.
- Tardy, Y., Nahon, D., 1985. Geochemistry of laterites, stability of Al-goethite, Al-hematite, and Fe³⁺-kaolinite in bauxites and ferricretes – An approach to the mechanism of concretions formation. *Am. J. Sci.* 285 (10), 865–903.
- Thomas-Keprta, K.L., Clemett, S.J., Bazylinski, D.A., Kirschvink, J.L., McKay, D.S., Wentworth, S.J., Vali, H., Gibson, E.K., McKay, M.F., Romanek, C.S., 2001. Truncated hexa-octahedral magnetite crystals in ALH84001: presumptive biosignatures. *Proc. Natl. Acad. Sci. U. S. A.* 98 (5), 2164–2169.
- Till, J., Guyodo, Y., Lagroix, F., Morin, G., Ona-Nguema, G., 2015. Goethite as a potential source of magnetic nanoparticles in sediments. *Geology* 43 (1), 75–78.
- Till, J.L., Jackson, M.J., Moskowitz, B.M., 2010. Remanence stability and magnetic fabric development in synthetic shear zones deformed at 500 °C. *Geochem. Geophys. Geosyst* 11 (12) , <http://dx.doi.org/10.1029/2010GC003320>.
- van der Zee, C., Roberts, D.R., Rancourt, D.G., Slomp, C.P., 2003. Nanogoethite is the dominant reactive oxyhydroxide phase in lake and marine sediments. *Geology* 31 (11), 993–996.
- Verwey, E.J., 1939. Electronic conduction of magnetite (Fe₃O₄) and its transition at low temperature. *Nature* 144, 327–328.
- Wang, H., Kent, D.V., Jackson, M.J., 2013. Evidence for abundant isolated magnetic nanoparticles at the Paleocene–Eocene boundary. *Proc. Natl. Acad. Sci. U. S. A.* 110 (2), 425–430.
- Wang, H.P., Wang, J., Chen-Wiegart, Y.C.K., Kent, D.V., 2015. Quantified abundance of magnetofossils at the Paleocene–Eocene boundary from synchrotron-based transmission X-ray microscopy. *Proc. Natl. Acad. Sci. U. S. A.* 112 (41), 12598–12603.
- Weiss, B.P., Kim, S.S., Kirschvink, J.L., Kopp, R.E., Sankaran, M., Kobayashi, A., Komeili, A., 2004a. Ferromagnetic resonance and low-temperature magnetic tests for biogenic magnetite. *Earth Planet. Sci. Lett.* 224, 73–89.
- Weiss, B.P., Kim, S.S., Kirschvink, J.L., Kopp, R.E., Sankaran, M., Kobayashi, A., Komeili, A., 2004b. Magnetic tests for magnetosome chains in Martian meteorite ALH84001. *Proc. Natl. Acad. Sci. USA* 101 (22), 8281–8284.
- Whicker, J.J., Breshears, D.D., Wasiolek, P.T., Kirchner, T.B., Tavani, R.A., Schoep, D.A., Rodgers, J.C., 2002. Temporal and spatial variation of episodic wind erosion in unburned and burned semiarid shrubland. *J. Environ. Qual.* 31 (2), 599–612.